Summer upwelling in the South China Sea and its role in regional climate variations

Shang-Ping Xie
International Pacific Research Center and Department of Meteorology, University of Hawaii, Hawaii, USA

Qiang Xie and Dongxiao Wang
LED, South China Sea Institute of Oceanology, Chinese Academy of Sciences, Guangzhou, China

W. Timothy Liu
Jet Propulsion Laboratory, Pasadena, California, USA

Received 21 March 2003; revised 15 May 2003; accepted 27 May 2003; published 14 August 2003.

[1] Seasonal and interannual variations of summer upwelling off the South Vietnam coast and the offshore spread of cold water are investigated using a suite of new satellite measurements. In summer, as the southwesterly winds impinge on Annam Cordillera (a north-south running mountain range on the east coast of Indochina) a strong wind jet occurs at its southern tip offshore east of Saigon, resulting in strong wind curls that are important for ocean upwelling off the coast. In July and August an anticyclonic ocean eddy develops to the southeast, advecting the cold coastal water offshore into the open South China Sea (SCS). The center of this cold filament is located consistently north of the wind speed maximum, indicating that open-ocean upwelling helps to cool the ocean surface. Corroborating evidence for the cold filament is found in ocean color observations that reveal a collocated tongue of high chlorophyll concentration. The development of this cold filament disrupts the summer warming of the SCS and causes a pronounced semi-annual cycle in SST. Moreover, the cold filament is an important player in interannual variability in the summer SCS. In 1998, the cold filament and mid-summer cooling never took place, giving rise to a strong basin-wide surface warming. Interannual SST variance has a local maximum over the climatological cold filament, and is much greater than the variance over the adjacent Indian and western Pacific Oceans. A cold filament index is constructed, which displays significant lagged correlation with SST in the eastern equatorial Pacific and Indian Oceans, indicative of a teleconnection from El Nino. *INDEX TERMS:* 4504 Oceanography: Physical: Air/sea interactions (0312); 4279 Oceanography: General: Upwelling and convergences; 4243 Oceanography: General: Marginal and semienclosed seas; 4215 Oceanography: General: Climate and interannual variability (3309); *KEYWORDS:* upwelling, air-sea interaction, orographically induced wind jet, ocean stationary eddy, South China Sea, climate variability

Citation: Xie, S.-P., Q. Xie, D. Wang, and W. T. Liu, Summer upwelling in the South China Sea and its role in regional climate variations, *J. Geophys. Res.*, *108*(C8), 3261, doi:10.1029/2003JC001867, 2003.

1. Introduction

[2] The South China Sea (SCS) is a large semi-enclosed marginal ocean basin with a total area of 3.5 million km^2 and an average depth of over 2000 m (Figure 1a). It is connected with the East China Sea to the northeast, the Pacific Ocean and the Sulu Sea to the east, and the Java Sea and the Indian Ocean to the southwest. SCS climate is part of the East Asian monsoon system [*Wyrtki*, 1961; *Lau et al.*, 1998]. In this paper, seasons always refer to those for the Northern Hemisphere; summer, for example, refers to June, July, and August. In winter the SCS is dominated by the strong northeasterly monsoon, whereas in summer the winds reverse direction to southwesterly [e.g., *Liu and Xie*, 1999]. From spring to summer, sea surface temperature (SST) in the SCS does not increase monotonically with solar radiation at the top of the atmosphere, but begins to decrease after the onset of the southwest monsoon, giving rise to a pronounced semi-annual cycle in SST. The present study investigates the mechanism for this basin-scale mid-summer cooling and shows that wind-induced upwelling and other ocean dynamic processes are important.

[3] Previous studies have shown that upwelling takes place off the Vietnamese coast in summer during the southwest monsoon. *Wyrtki* [1961] was among the first to point out this seasonal upwelling and showed that there is a more than 1°C drop in SST off Vietnam in summer [see also *Huang et al.*, 1994]. *Kuo et al.* [2000] observed upwelling along the western coast of the SCS using Advanced Very

0148-0227/03/2003JC001867$09.00

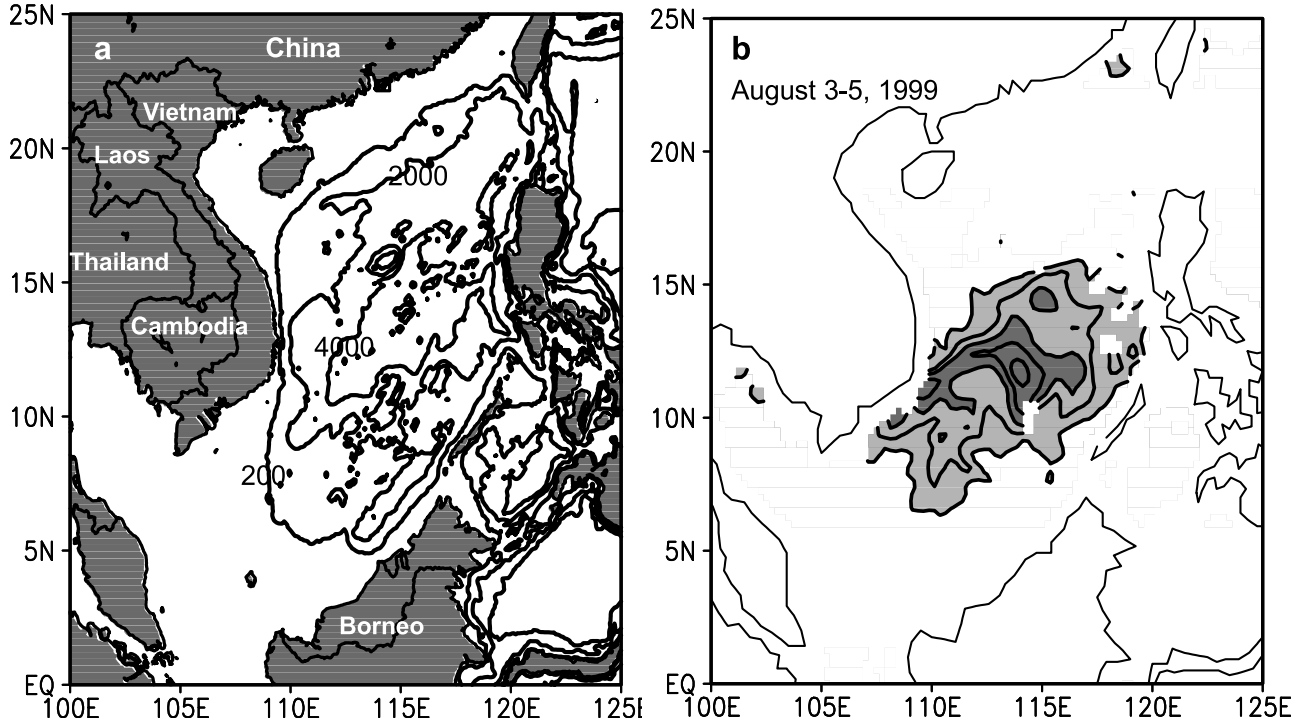

Figure 1. (a) Bathymetry of the South China Sea, with only the 200, 2000, and 4000 m contours plotted. (b) TMI SST averaged for August 3–5, 1999. Contour intervals are 0.5°C, with dark and light shade denoting SST below 27°C and 28°C, respectively.

High Resolution Radiometer (AVHRR) infrared images for the 1996 and 1997 summers, and found that the cold water on the coast extended offshore and evolved into a cold jet stretching eastward along 11°N–12°N in mid-August 1997. *Xu et al.* [1982] and *Ho et al.* [2000b] showed that there is a region of relatively low sea surface height (SSH) off South Vietnam indicative of the occurrence of upwelling. This SSH low seems to be consistent with a thermocline dome off South Vietnam at about 12°N that was captured by an airborne Expendable Bathythermography (XBT) survey in May 1995 [*Chu et al.*, 1998]. Forced by observed winds, several models were able to produce the summer upwelling and SST cooling off the Vietnamese coast [*Pohlmann*, 1987; *Shaw and Chao*, 1994].

[4] In the rest of this paper, we call the eastward extension of cold surface water from the Vietnamese coast the "cold filament." Figure 1b shows a 3-day mean SST map in August 1999 that features such a cold filament with minimum SST below 26°C in the open SCS. *Kuo et al.* [2000] speculated that the current structure and the cold filament might be related, but without further discussing the mechanism. Surface dynamic height derived from hydrographic measurements and SSH observations by TOPEX/POSEIDON (T/P) satellite altimeter agree that on the basin scale, there is an anticyclonic circulation in summer with maximum SSH located west of Luzon Island [*Qu*, 2000; *Ho et al.*, 2000b; *Yang et al.*, 2002], but the regional circulation east of South Vietnam, which is likely to be important for the cold filament, is not well described nor understood. Earlier hydrographic observations suggest stationary eddies there [*Xu et al.*, 1982], but recent SSH analyses based on in situ and satellite observations seem to disagree [*Qu*, 2000; *Ho et al.*, 2000b]. Large disagreements also exist among ocean general circulation models (GCMs) on regional circulation east of Vietnam [*Yang et al.*, 2002; *Wei et al.*, 2003], probably because of the differences in wind-forcing used. *Xie et al.* [2002a] computed the Sverdrup transport function based on several wind products and reported large differences among them, especially in the central SCS.

[5] The cold filament east of South Vietnam is the focus of this study. Previous studies of SCS circulation relied on sparsely distributed ship and/or T/P measurements, which are not suitable for studying narrow features such as the cold filament. The use of high-resolution AVHRR observations, on the other hand, was limited to a few case studies because of extensive clouds in the southwest monsoon season. These limitations on spatial resolution and temporal sampling leave open several important questions: Does this filament exist every summer and what are the key processes to its offshore development?

[6] The present study attempts at a systematic description of the seasonal evolution of the mid-summer cooling in the SCS and the ocean-atmospheric processes that give rise to this phenomenon. The use of new high-resolution satellite observations that became available only a few years ago is a unique feature of this study. In particular, the Tropical Rain Measuring Mission (TRMM) satellite's microwave imager (TMI) can see through clouds and substantially improve the sampling of SST over cloudy regions like summer SCS [*Wentz et al.*, 2000; *Xie et al.*, 2001]. Blending altimetry measurements made by the co-orbiting European Remote Sensing (ERS) and T/P satellites significantly increases their spatial resolution, making them suitable for studying stationary eddies in SCS. In addition, we will use high-

resolution satellite observations of surface wind and relate the wind-forcing with observed circulation and SST distribution in SCS.

[7] SCS SST experiences significant interannual variability in summer that is correlated with eastern Pacific SST at a half-year lag [*Ose et al.*, 1997; *Wang et al.*, 2000b]. In 1998, for example, the SCS is anomalously warm, making it the warmest summer on record in this region [*Wang et al.*, 2002]. Given its prominence in the SCS seasonal cycle, does the cold filament play a role in interannual variability on the basin scale? If so, what causes interannual variability in the cold filament? What is the relationship between this cold filament and larger-scale variability over the Pacific and Indian Oceans?

[8] This paper is a synthesis of elements of SCS summer climate and its variability by taking advantage of new satellite observations of the ocean and atmosphere. We find that on the climatological mean, the cold filament develops from the Vietnam coast eastward to the open SCS from June to August. On the basis of analysis of these new satellite data, a conceptual model is presented that traces the origin of the cold filament, surprisingly, to mountains on Indochina. We show that the cold filament displays large interannual variability in association with changes in the atmospheric and the SCS ocean circulations. A cold filament index is constructed, and its correlation with global variability indicates that the summer SCS variability is closely related to Pacific El Niño/Southern Oscillation (ENSO) and the attendant anomalous high-pressure system in the western Pacific atmosphere.

[9] The rest of the paper is organized as follows. Section 2 describes the data sets. Section 3 presents the seasonal evolution of the coastal upwelling and its eastward extension. Section 4 defines a cold filament index and investigates its correlation with global variability. Section 5 is a summary.

2. Data

[10] This study analyzes a suite of satellite observations of SST, SSH, sea surface wind, and chlorophyll by several satellite sensors on different platforms. These new satellite observations offer a view of the vast oceans and the overlying atmosphere never possible before, and their combined analyses have led to a burst of air-sea interaction studies [*Xie et al.*, 1998; *Wentz et al.*, 2000; *Liu et al.*, 2000; *Chelton et al.*, 2001a; *Hashizume et al.*, 2001; *Xie et al.*, 2001; *Nonaka and Xie*, 2003]. S.-P. Xie (Satellite observations of cool ocean-atmosphere interaction, submitted to *Bulletin of the American Meteorological Society*, 2003) provides a latest review of these new satellite studies.

[11] Using microwave sensors, TMI measures SST and surface wind speed nearly free of cloud influence over the global tropics within 38°N/S, at resolutions of 0.25° in space and 2∼3 days in time [*Wentz et al.*, 2000]. Here we use a monthly product available since December 1997 on a 0.25° grid. We supplement this TMI data set with a SST climatology on a 9-km grid that is based on AVHRR observations for a 15-year period of 1985–1999 [*Armstrong and Vazquez-Cuervo*, 2001]. AVHRR complements TMI observations in covering a longer period of time and coastal waters where TMI measurements are contaminated by land microwave emission.

[12] Altimeters on the ERS and T/P satellites measure SSH deviations from the long-term mean at their nadir. There is a tradeoff between spatial and temporal resolution: T/P has a 10-day repeat orbit with a zonal spacing between ground tracks of about 3° at SCS's latitudes, while these numbers are 35 days and 0.7° for ERS [*Chelton et al.*, 2001b]. We use a merged SSH data set that takes advantage of both T/P's high temporal and ERS's high spatial resolutions [*Ducet et al.*, 2000], available from October 1992 to July 2001 on a 0.25° grid. Monthly means are used.

[13] The Sea-viewing Wide Field-of-view Sensor (SeaWiFS) satellite measures ocean color and chlorophyll concentration since October 1997, which are often a good indicator of ocean upwelling. We use the monthly averages on a 0.25° grid.

[14] The microwave scatterometer on the QuikSCAT satellite measures surface wind velocity over the world ocean on a daily basis [*Liu et al.*, 2000]. We construct a monthly climatology of wind stress from daily QuikSCAT observations for August 1999 to November 2002 on a 0.25° grid. While having lower resolutions in space and time than QuikSCAT, ERS scatterometers operate for a longer period of time, allowing us to study interannual variability in SCS. We use a monthly mean ERS wind stress data set on a 1° grid from September 1991 to December 2000.

[15] Most of the above satellite observations are not available prior to early 1990s. To obtain robust statistics of interannual variability, we use the following coarser-resolution observations/analyses. For SST, we use the *Reynolds and Smith* [1994] analysis available at 1° resolution. We limit our interannual variability analysis to after 1982, the year when satellite infrared SST observations became operational. For surface wind and sea level pressure (SLP), we use the NCEP-NCAR reanalysis on a 1.9° grid [*Kalnay et al.*, 1996]. For precipitation, we use the monthly precipitation anomalies derived from the Climate Prediction Center Merged Analysis of Precipitation (CMAP) data set [*Xie and Arkin*, 1996], available from 1979.

[16] In general, signals to be discussed are well above measurements errors. We refer to relevant references in the above for satellite-data error analysis. For our analysis, we use several independent measurements, which turn out to yield mutually corroborating and physical consistent results. Such physical consistency gives us confidence in the analysis results.

3. Seasonal Evolution

[17] This section describes the evolution of the ocean-atmosphere system in the summer SCS. We begin with an examination of surface winds, which are key to understanding both SST and ocean circulation.

3.1. Prevailing Winds and Land Orographic Effect

[18] On average, the seasonal transition from the northeast to southwest monsoon occurs in May [*Lau et al.*, 1998]. In summer, the southwesterly winds prevail in SCS. Figure 2 displays the climatological distribution of QuikSCAT wind stress for June–August. At about 10°N off Vietnam, the southwesterly wind stress reaches a maximum ($\sim$0.18 Nm^{-2}) that is twice as strong as in the ambient. While this wind jet is present in several other ocean wind

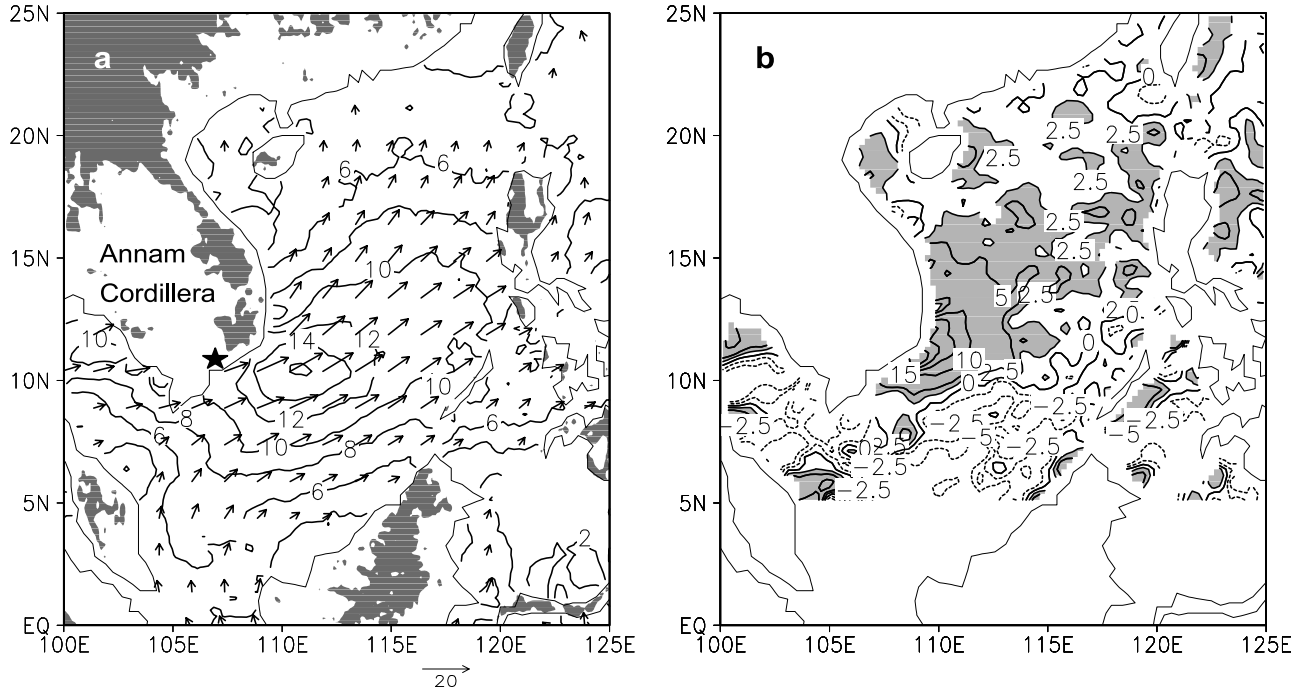

Figure 2. (a) QuikSCAT surface wind stress vectors and their magnitude (contours in 10^{-2} Nm^{-2}) averaged for June–August 2000–2002. (b) Ekman pumping velocity (upward positive in 10^{-6} m/s; contour intervals are 2.5 for values between −5 and 5, and are otherwise 5, with values greater than 2.5 shaded). In Figure 2a, land topography with elevations greater than 500 m is shaded and the star marks the location of Saigon.

products [*Xie et al.*, 2002a], its cause has not been discussed in literature.

[19] Land topography with elevations greater than 500 m is shaded in Figure 2a. Annam Cordillera is a mountain range that rises above 500 m and runs in a north-south direction on the east coast of Indochina Peninsula on the Vietnam-Laos/Cambodia borders and ends just north of Ho Chi Minh City (also known as Saigon: 106°41′, 10°47′; marked by a star symbol in Figure 2a). The southwesterly winds are blocked by these mountains and are weak over the ocean to the east. At the southern tip of this mountain range, on the other hand, winds rush through, forming a strong wind jet offshore east of Saigon. Results from a high-resolution (0.1° in horizontal), full-physics regional atmospheric model of Y. Wang et al. (Regional model simulations of marine boundary layer clouds over the Southeast Pacific off South America: I. Control experiment, submitted to *Monthly Weather Review*, 2003) support this orographic-effect hypothesis. In an experiment that removes the mountains on Indochina, the southwesterlies become much more uniform in the meridional direction and the wind jet offshore disappears (H. Xu, personal communication, 2003).

[20] The axis of this wind jet divides the SCS into two parts, with Ekman upwelling and downwelling prevailing in the northern and southern parts, respectively (Figure 2b). The rest of this paper demonstrates that this wind jet is very important for SCS ocean circulation, biological activity and regional climate variability.

3.2. SST and Cold Filament

[21] The coast of South Vietnam is oriented in a southwest to northeast direction, roughly in parallel with the prevailing southwesterly winds. By the mechanism of coastal upwelling, the alongshore wind can easily pump the cold water from beneath the mixed layer to the surface along the south Vietnam coast (Figure 3a). The maximum coastal cooling takes place just east of Saigon, coinciding roughly with the wind speed maximum along the coast. While previous research emphasizes the coastal upwelling induced by alongshore winds that are assumed to be uniform in the offshore direction [*Kuo et al.*, 2000], high-resolution QuikSCAT observations reveal an intense open-ocean Ekman pumping (>2 m/day) associated with a strong offshore increase in southwesterly winds (Figure 2b). This offshore upwelling appears to be important in causing the strongly localized cooling on the coast east of Saigon.

[22] After being initiated in June, the cold water does not just stay on the coast but spreads eastward over most of the central SCS in July and August (Figures 3b and 3c). The northeastward oriented cold filament reaches its maximum intensity (minimum temperature) in August, with a larger width in this 15-year AVHRR climatology than in the snapshots of *Kuo et al.* [2000] and Figure 1b because of large temporal variability (section 4). Associated with this narrow filament is a basin-wide cooling that progresses from July onward. By August, SST is 0.5°C or more below that in June over most of the SCS except near the Chinese coast.

3.3. Role of Ocean Dynamics

[23] While evaporative cooling induced by the intensifying southwest monsoonal winds is probably important for the basin-scale cooling in the mid-summer [*Qu*, 2001], this subsection considers other possible mechanisms for the eastward development of the cold filament, such as geo-

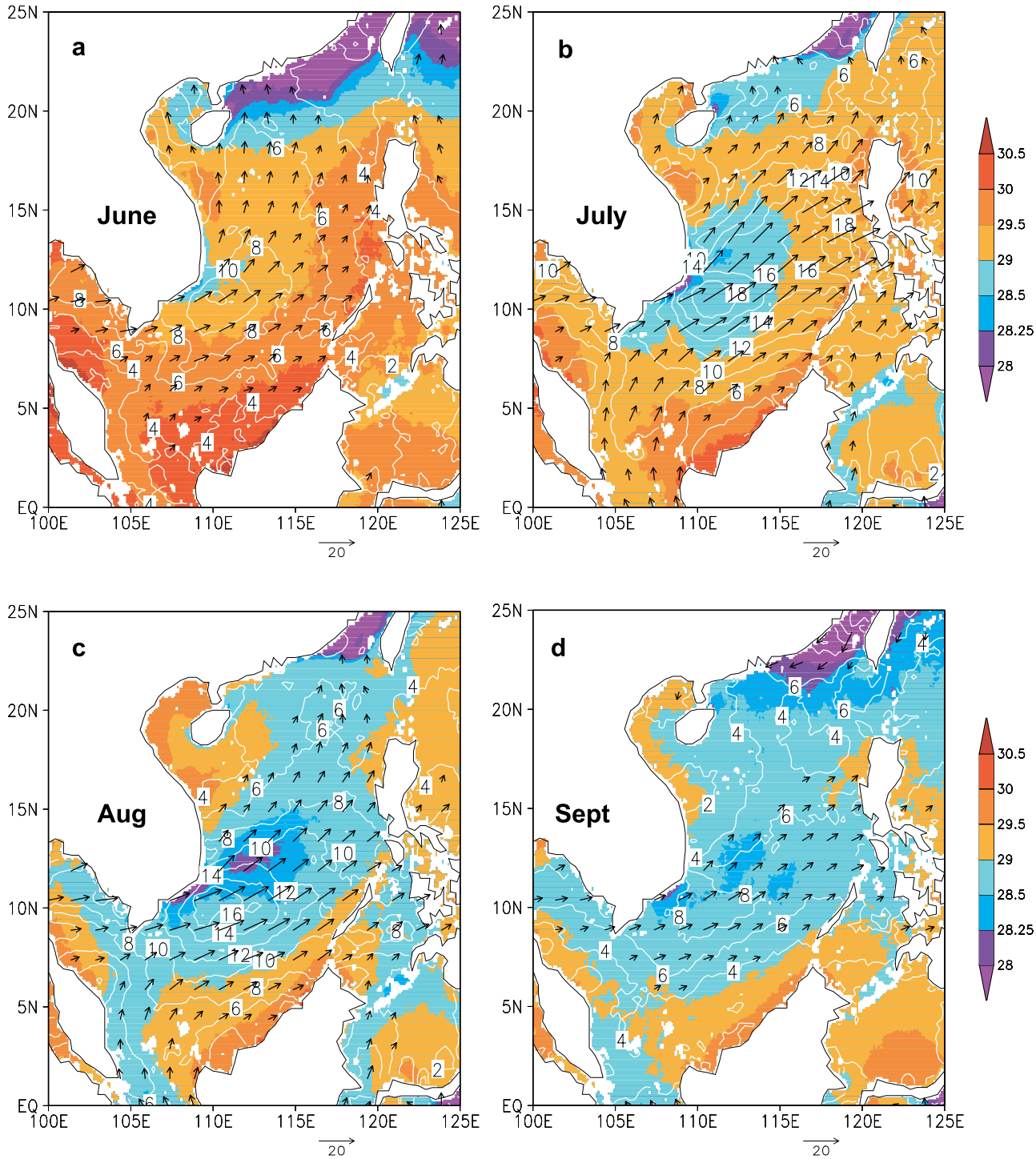

Figure 3. AVHRR SST climatology (color shade in °C), along with QuikSCAT surface wind vectors and magnitude (contours in 10^{-2} Nm^{-2}).

strophic advection and open-ocean upwelling, and test them against satellite observations in a qualitative manner. A quantitative estimate of ocean heat budget is beyond the scope of this study and a subject of our future study.

[24] Figure 4 shows the 8-year (1993–2000) SSH climatology superimposed on SST in July and August. There is a strong anti-cyclonic eddy east of Saigon centered at 112°E, 10°N that is stronger in August than in July. Separated from this southern high by a streak of SSH minimum, there is another meridional SSH maximum further to the north at 16°N that weakens from July to August. This double anticyclonic circulation is broadly consistent with the *Xu et al.* [1982] hydrographic observations and is noted by *Kuo et al.* [2000] in satellite SSH snapshots of August 1997, suggesting that it is indeed a recurring climatological feature of the SCS circulation system in summer. Hereinafter, we call the southern anti-cyclonic eddy east of Saigon the "South Vietnam (SV) Eddy." This SV eddy is clearly

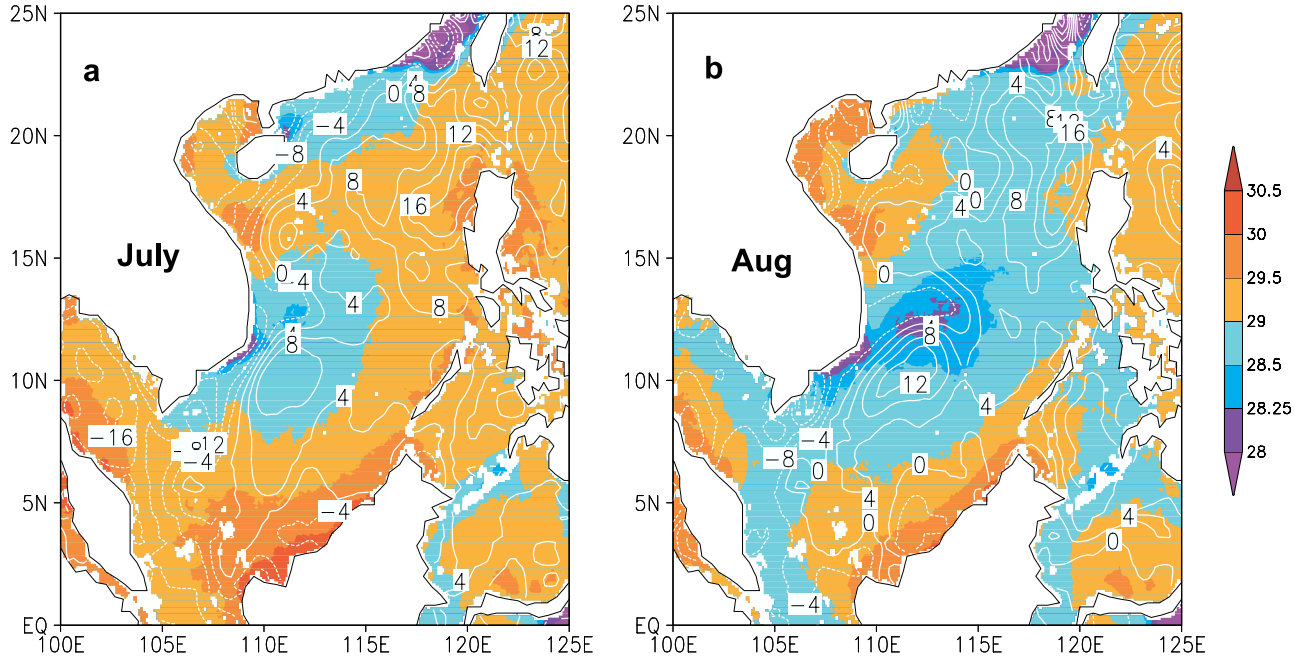

Figure 4. SSH climatology based on merged satellite observations (contours in cm), and AVHRR SST climatology (color shade in °C).

visible in hydrographic and ADCP current measurements in July 1999 [*Fang et al.*, 2002]. The SV Eddy appears to be forced by the Ekman downwelling on the southern flank of the wind jet (Figure 2b), but probably not by the simple Sverdrup gyre mechanism. This anticyclonic eddy seems highly nonlinear, with the maximum surface current velocity amounting to 0.5 m/s on its northern flank based on a geostrophic calculation using this 8-year climatology of SSH. The eddy and its circulation are likely to be even stronger in individual years. The eastward current speed exceeds 1 m/s in a July 1999 ADCP survey [*Fang et al.*, 2002, Figure 6]. We suggest an analogy to the Great Whirl off the Somali coast that forms under the strong southwest monsoon and involves both strong nonlinear interaction of the eddy with mean flow and coastal orographic effect on surface winds. (See *Schott and McCreary* [2001] for a review of Great Whirl research in the Arabian Sea.) This analogy needs to be tested and further explored in high-resolution numerical models.

[25] The strong northeastward current northwest of the SV Eddy advects the cold coastal water east of Saigon offshore. Indeed, in August, the center of the cold filament roughly coincides with the maximum offshore currents associated with the eddy up to 113°E (Figure 4b). Farther to the east, the cold water shows a tendency to spread southward on the eastern flank of the SV Eddy where the

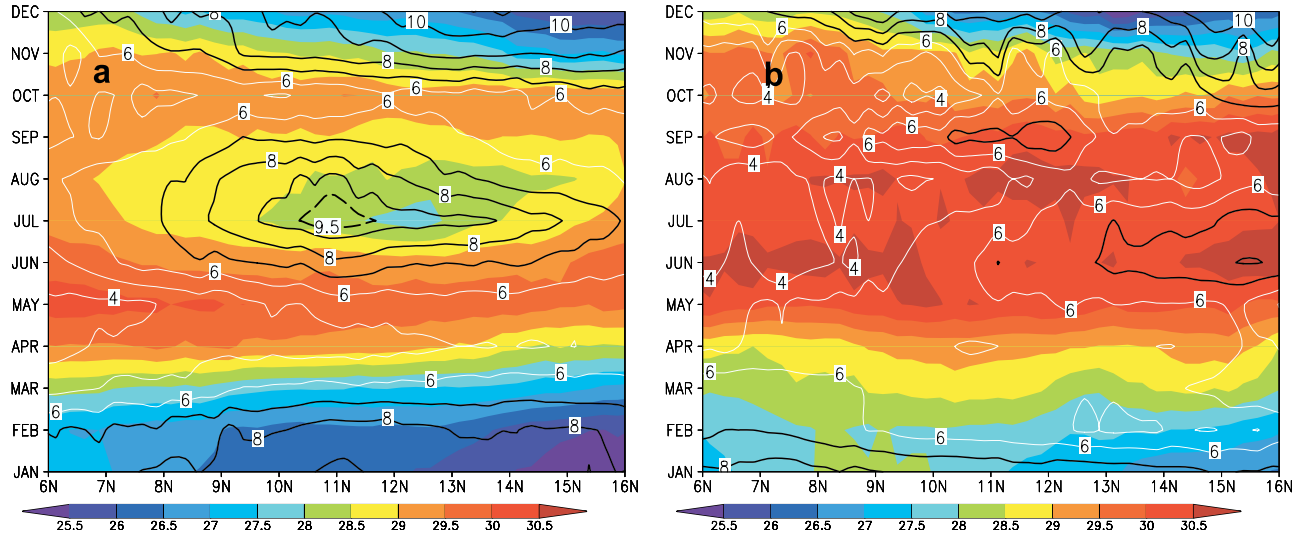

Figure 5. Latitude-time sections of TMI SST (shaded in °C) and wind speed (contours in m/s) along 112°E: (a) averaged for 1999–2002 and (b) for 1998. High wind speeds (>7m/s) are highlighted in black contours.

eddy flow starts to turn toward the south. This eddy-advective effect is better seen in the snapshot in Figure 1b that captures the south turn of the cold filament in the mid-basin.

[26] Part of the cold filament, while diffused and patch-like, continues to extend northeastward beyond 113°E, in the general direction of the wind jet. A closer inspection of Figure 3c indicates that the center of the cold filament is consistently displaced northward of the wind jet axis, a fact inexplicable from wind-induced evaporative cooling. The maximum evaporative cooling occurs along the wind jet axis, and the resultant SST minimum would be displaced instead to the south considering the advection by the southeastward Ekman flow at the surface. Therefore we suggest that the open-ocean upwelling on the northern flank of the southwest wind jet contributes to the continued eastward expansion of the cold filament, interpreting the observed northward displacement of the cold filament relative to the wind jet as the corroborating evidence.

[27] Figure 5a shows the latitude-time section along 112°E of TMI SST and wind speed averaged for 1999–2002. SCS SST reaches a minimum in winter under the strong northeasterly monsoon. From January, the SCS begins to warm up as the northeast winter monsoon relaxes and solar radiation increases, reaching a SST maximum in May just before the onset of the southwest monsoon. As the southwest monsoon intensifies, SST plummets and reaches a minimum in July/August. SST recovers thereafter and reaches another maximum in October. The southwesterly wind-induced cold filament is the cause of the mid-summer cooling in SCS, resulting in a pronounced semi-annual cycle in SST despite a strong annual cycle in local solar radiation at the top of the atmosphere. We note again that the center of the mid-summer cooling is displaced about 200 km north of the wind maximum, indicative of ocean dynamic effects other than surface Ekman advection.

3.4. Chlorophyll

[28] Rich nutrients in upwelling zones often support active biological activity. Thus chlorophyll is a useful indicator for ocean upwelling. Figure 6 displays the 4-year (1999–2002) climatology of SeaWiFS chlorophyll concentration for June–August. In general, chlorophyll concentration greater than $10^{-0.5}$ mg/m^3 (shaded red) is almost exclusively confined to shallow waters with depths less than 50 m. A noticeable exception is a region northeast of Saigon where high chlorophyll penetrates into the deep open ocean, apparently consistent with the offshore advection by the stationary SV Eddy as discussed above. In addition, this high-chlorophyll tongue is also roughly collocated with strong Ekman upwelling. The relative importance of geostrophic advection and local upwelling for this high-nutrient tongue needs to be determined from observations and numerical simulations.

3.5. A Conceptual Model

[29] On the basis of the above analysis, we propose a conceptual model for the eastward-extending cold filament. As the southwest monsoonal winds impinge on the mountain range on the east coast of Indochina Peninsula, the orographic blockage accelerates the winds on the southern tip of Annam Cordillera, leading to the formation of a strong wind jet offshore. This wind jet initiates the coastal upwelling and causes the mid-summer cooling on the basin scale by the following mechanisms. First, the Ekman downwelling on the southern flank of the wind jet forces a quasi-stationary anticyclonic eddy in the ocean, which advects the cold coastal water to the east. Offshore, the strong winds cause strong evaporative cooling to sustain the northeastward spread of cold water. Finally, the open-ocean Ekman upwelling on the northern flank of the wind jet is an additional mechanism for offshore cooling, keeping the SST minimum displaced north of the wind speed maximum. This conceptual model casts the mountain range and its orographic blockage as the ultimate cause of the upwelling cooling both on the coast and in the open SCS. A key element of this conceptual model, the wind-forcing of the anticyclonic SV Eddy, is still hypothetical at this stage and requires further study.

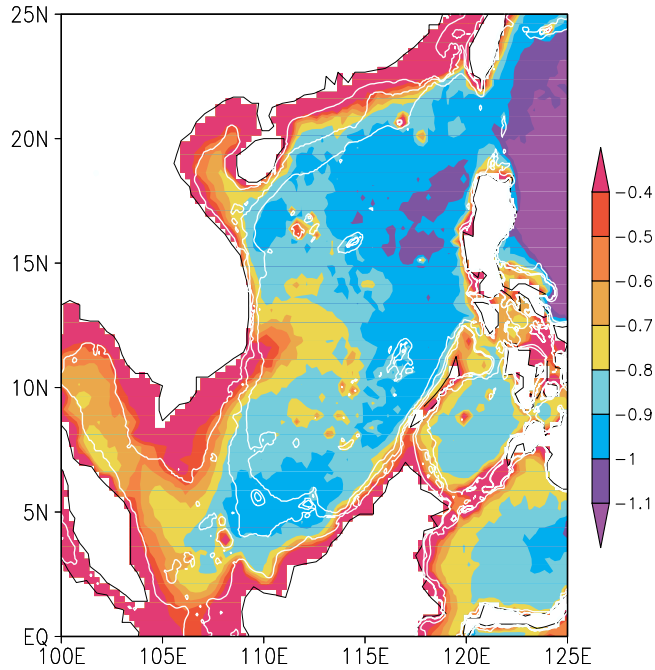

Figure 6. Logarithm (Log_{10}) of SeaWiFS chlorophyll concentration averaged for July–August 1999–2002 (color shade in mg m^{-3}), along with bottom topography contours for 50, 100, and 500 m.

4. Interannual Variability

4.1. 1998 Warm Event

[30] A strong warm event takes place and lasts for the entire year of 1998 [*Wang et al.*, 2002]. Figure 5 contrasts SST and wind speed between a normal and this anomalous warm year based on TMI observations. In January 1998, SST along 112°E is already 2°C or more above the climatology. The SCS remains abnormally warm and wind speed abnormally weak throughout 1998. In particular, the mid-summer cooling never takes place in 1998. In the 10°N–14°N band that normally the summer cold filament occupies, SST continues to increase in summer and peaked in August 1998.

[31] Here we use the 1998 summer event to illustrate the role of the cold filament in regional climate variability. The

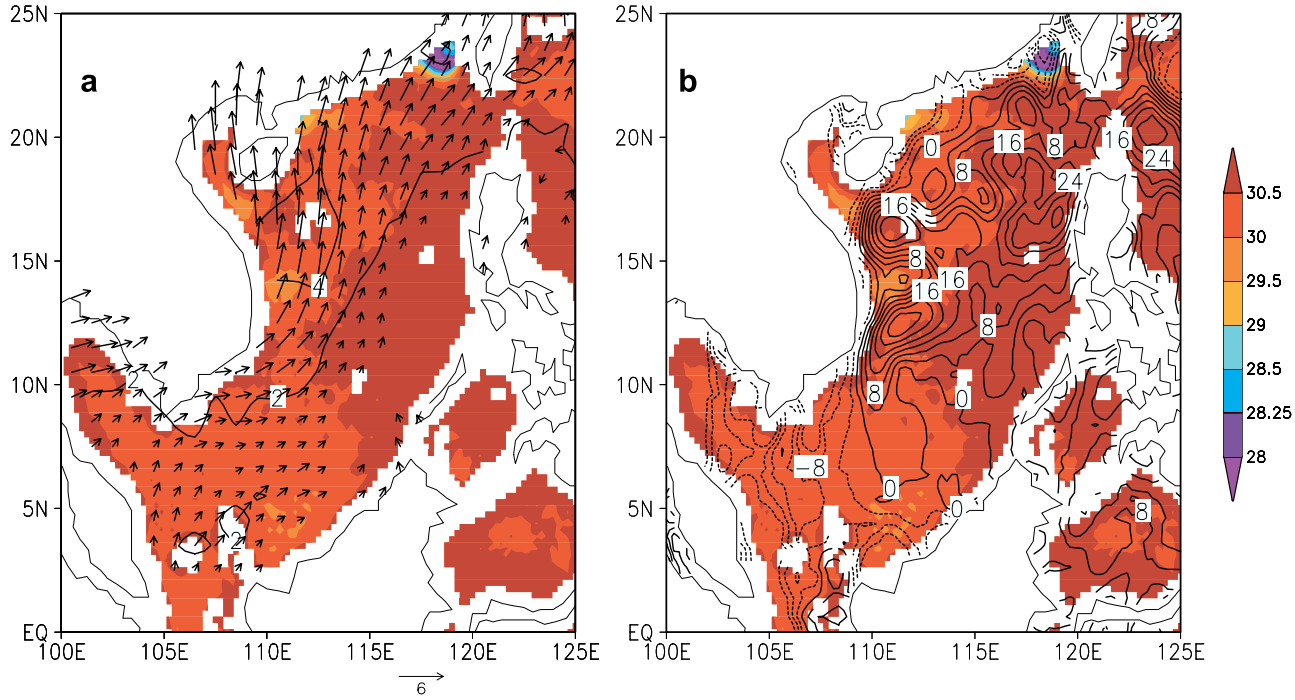

Figure 7. TMI SST (shaded in °C), (a) wind stress (10^{-2} Nm^{-2}) and (b) SSH (contours in cm) averaged for July–August 1998. Note that the scale for wind stress vectors is 3.3 times smaller than in Figures 2 and 3.

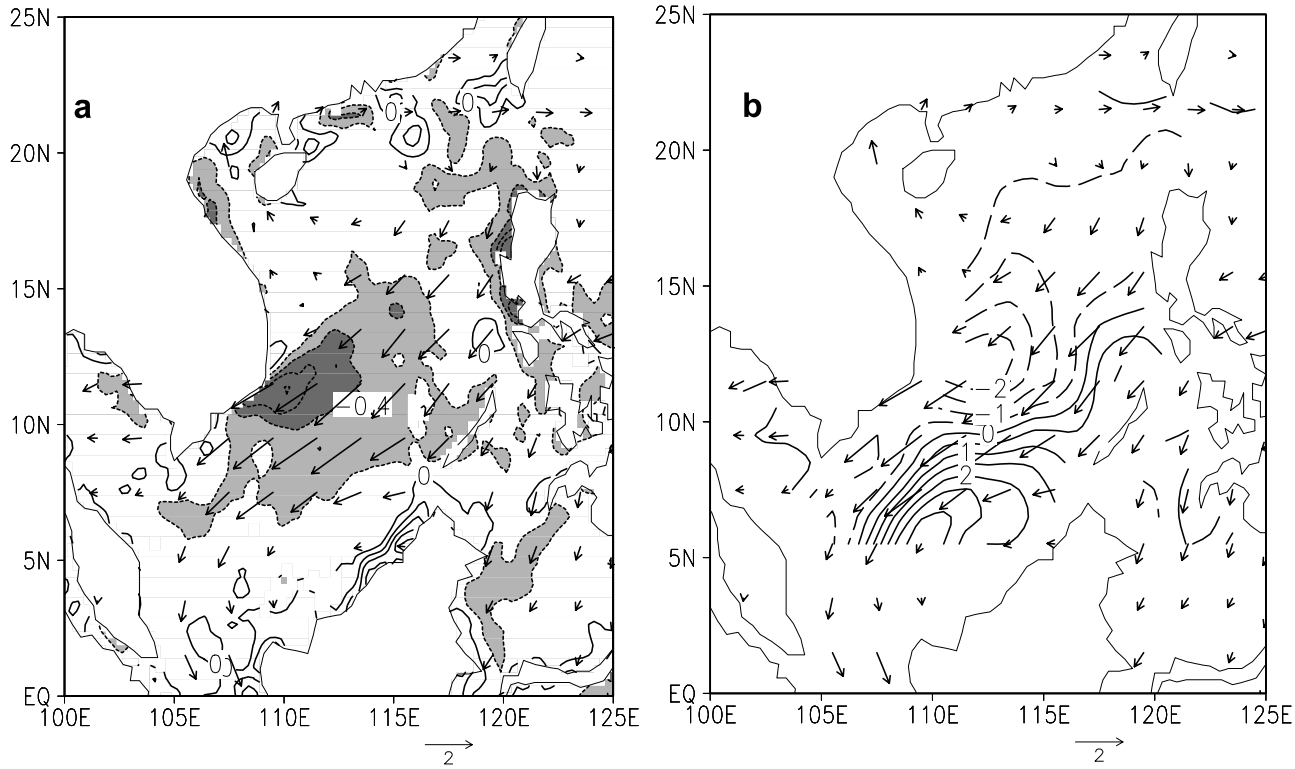

Figure 8. The 1998 difference from the climatological mean, averaged for July–August: ERS wind stress vectors; (a) logarithm of SeaWiFS chlorophyll concentration (mg m^{-3}); and (b) Ekman pumping velocity (10^{-6} ms^{-1}). The climatological means are based on 1999–2002 for chlorophyll and 1992–2000 for ERS wind.

wind speed decreases by more than half in 1998 summer (Figures 5b and 7), especially in the central basin. (Note that the wind stress scale in Figure 7 is reduced by a factor of 3.3 relative to Figure 2.) The wind stress vectors shift into southerly, more or less along the shore off Vietnam, a direction that minimizes the aerodynamic effect of Annam Cordillera. The wind jet east of Saigon is nowhere to be seen, and neither is the cold filament in the ocean. Ocean circulation also experiences large changes. In particular, the anticyclonic SV Eddy is squashed in the meridional direction and moves northward by 200–300 km. Off Saigon (110°E, 11°N), the normal offshore flow reverses its direction and is replaced with an onshore current, preventing the offshore spread of coastal water there. SCS SST remains nearly uniform and anomalously high through the summer 1998. Thus the great summer warming of 1998 may be viewed as resulting from the diminished wind jet offshore and suppressed mid-summer cooling.

[32] Figure 8 shows the chlorophyll difference between 1998 and 1999–2002 climatology, along with anomalies of ERS wind stress and Ekman pumping in 1998. Compared with normal years of 1999–2002, chlorophyll concentration shows a basin-wide decrease in 1998 summer. Large chlorophyll decrease is found along the path of the climatological cold filament, roughly coinciding with a region of anomalous Ekman downwelling in the ERS observations. Maximum chlorophyll decrease is found on and off the coast east of Saigon, corroborating the key role of the wind jet in maintaining upwelling there in normal years. The diminished wind jet there results in a large downwelling anomaly offshore in 1998 (Figure 8b).

4.2. Statistic Analysis

[33] As the 1998 warm event illustrates, SCS experiences considerable interannual variability in summer. This and the next subsections investigate its time-space structure and relationships with other global-scale variability by systematic statistical analysis.

[34] Figure 9a depicts the root mean square (rms) variance of interannual SST variability in June–August based on the 1° × 1° Reynolds-Smith [*Reynolds and Smith*, 1994] analysis for a 21-year period of 1982–2002. There is a pronounced local maximum in the central SCS between 9°N–14°N that is roughly collocated with the climatological cold filament. At these latitudes, the RMS variance in the SCS is about 50% greater than that in the Indian Ocean to the west and the western Pacific to the east. In this latitude band, the NCEP/NCAR reanalysis for the same 21-year period (see Figure 9b) shows similar levels of wind speed variance in the SCS and western Pacific, suggesting that the ocean dynamics and cold filament play a role in producing the locally enhanced SST variance in SCS. (*Xie et al.* [2002b] show similar local enhancement of SST variance over tropical Indian Ocean upwelling zones where subsurface ocean variability is communicated to the surface effectively.)

[35] Figure 9c shows ERS wind speed RMS variance for the recent 9-year period. The relative strength of wind variance among the three oceans looks quite different between the ERS and reanalysis products. In the ERS observations, wind variance is much greater in the SCS than in the ocean either to the west and east, suggesting that the local

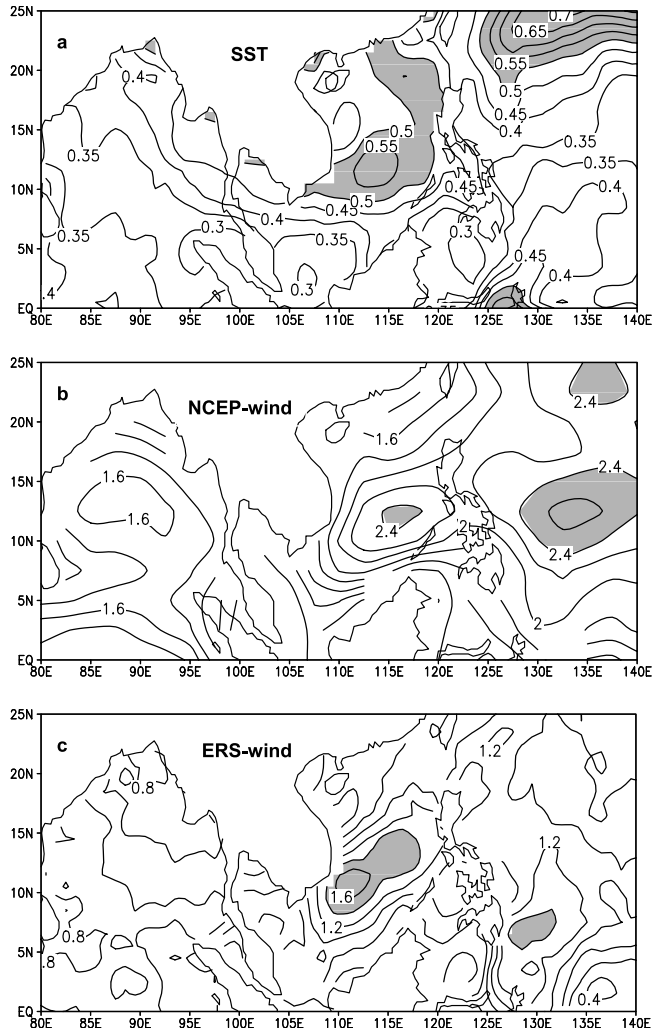

Figure 9. Rms of interannual variance averaged for June–August: (a) SST (K), surface wind speed (m/s) based on (b) NCEP reanalysis and (c) ERS observations.

wind-forcing, say through surface heat flux, is also important for high SST variance. Because of the coarse resolution (1.9°), the NCEP reanalysis may not resolve properly wind features in a small basin like the SCS, especially those induced by the mountain blockage. Satellite wind observations, though offering better resolution and not subject to model errors, are still too short for stable statistics. We have also computed the RMS variance for SST and wind speed using higher-resolution TMI observations for a 5-year period of 1998–2002 (not shown). The SST variance is more narrowly trapped along the climatological cold filament than in the Reynolds-Smith data set. In the western basin, this narrow TMI SST variance maximum is consistently displaced to the north of the wind speed variance maximum, corroborating the importance of the cold filament and the associated ocean dynamics in SCS SST variability.

[36] To further study the interannual variability, we define a cold filament index by averaging SST in the high variance region of 10°N–13°N, 110°E–118°E and for June–August. Figure 10a shows the correlations of CMAP rainfall, reanalysis SLP, and surface wind with this index. In

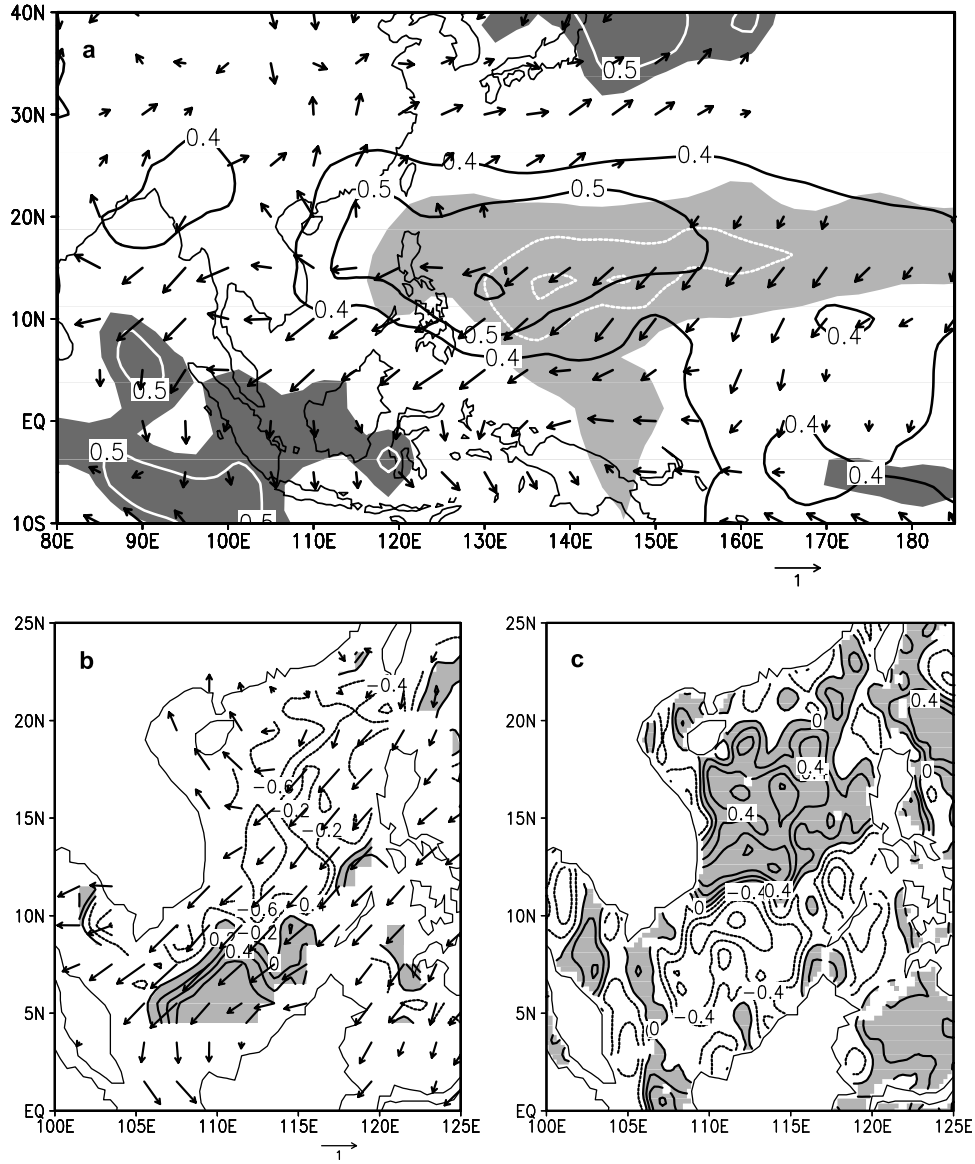

Figure 10. Simultaneous correlations with the summer SCS cold filament index for June–August: (a) NCEP sea level pressure (contours), surface wind velocity (vectors), and CMAP precipitation (light shade < 0.4 and dark shade > 0.4; white contours at 0.1 intervals); (b) ERS wind velocity (vectors) and Ekman pumping velocity (contours); and (c) SSH (contours).

a warm SCS event, convection and precipitation tend to be suppressed in the western North Pacific while enhanced over Japan, a teleconnection discussed by *Nitta* [1987]. There are positive precipitation anomalies over the eastern equatorial Indian Ocean, which *Annamalai et al.* [2003] suggest are associated with reduced convection over the western Pacific. The reduced northwestern Pacific monsoon rainfall results in a pronounced high-pressure center that strengthens the trade winds equatorward of 15°N. Anomalous northeasterly winds appear in the correlation field in the southern SCS (as can also be seen from ERS observations in more detail in Figure 10b).

[37] The SSH correlation field shows a dipole structure, positive in the northern and negative in the southern basin with the nodal line around 11°N (Figure 10c). SSH anomalies in the southern basin represent a marked weakening of the climatological anti-cyclonic circulation there, acting to inhibit the eastward advection of coastal water that is critical to the development of the cold filament in a normal year. East of Saigon, strong westward current anomalies are found in 10°N–12°N, which, according to the geostrophic calculation based on a SSH regression analysis, amount to a maximum of 0.72 m/s, a speed more than enough to reverse the eastward climatological flow (~0.5 m/s). This SSH dipole is consistent with the northward shift of the anti-cyclonic SV Eddy observed in 1998 summer.

[38] The wind shift is probably a cause of the SSH dipole. ERS wind observations indeed show anomalous Ekman downwelling and upwelling in the northern and southern basins, respectively, but the nodal line of the anomalous Ekman pumping is located around 9°N, about 3° to the south of the SSH nodal line. This discrepancy between the

wind-forcing and SSH response may be caused by ocean coastal waves and/or SSH variability from the western Pacific.

4.3. Correlation With Global Variability

[39] Figure 11 shows the summer cold filament index, along with the Nino3 SST index in January of the same year. The cold filament index is obviously correlated with ENSO at a half-year lag, with a correlation coefficient of 0.67 that is significant at the 95% level based on a t-test (assuming degree of freedom = 9). The intervals between warm events in SCS are 2–5 years, similar to those of El Nino.

[40] Figure 12 shows correlations with the summer cold filament index of Indo-Pacific SST, SLP and surface wind velocity 6 months ahead in January of the same year. The Pacific conditions are typical of an El Niño: positive SST correlations of up to 0.7 are found in the equatorial Pacific east of the dateline, accompanied by anomalous westerlies in the western equatorial Pacific. The Indian Ocean displays a warming pattern that is large south of the equator due to both ocean Rossby waves and wind-induced changes in surface heat flux [*Xie et al.*, 2002b]. There is a high-pressure system that occupies the entire western tropical North Pacific. This high pressure extends into the SCS, with westerly to southerly wind anomalies that blow against the prevailing northerly monsoon, giving rise to a winter warming in the SCS as took place in early 1998.

[41] Thus the summer SCS variability is highly correlated with Pacific ENSO and the attendant anomalous high-pressure system in the western Pacific atmosphere. While on average, Pacific ENSO peaks in boreal winter and then decays rapidly in spring, statistical analysis here shows that the western North Pacific high pressure persists into the summer following ENSO (Figure 10a). *Wang et al.* [2000a] propose that the interaction of this atmospheric anticyclonic circulation with the ocean mixed layer is responsible for its long persistence. Our results show that this persistent high pressure of the atmosphere strongly modulates the wind jet in the summer SCS, thereby inducing marked interannual variability there in ocean circulation, SST and plankton activity.

[42] The correlation with ENSO of changes in both basin-scale SSH and eddy-kinetic energy has been noted by *Ho et al.* [2000a] and *Hwang and Chen* [2000], respectively. These studies, however, have not considered the seasonal dependence of SCS interannual variability. Given the strong seasonal cycle that includes the reversal of prevailing winds, analyses based on seasonally stratified data are desirable. For example, the summer SSH-ENSO correlation distribution in Figure 10b is markedly different from *Ho et al.*'s [2000a] empirical orthogonal function mode of interannual variability in SSH, which is a mixture of winter and summer modes. While the delayed ENSO effect is a major mechanism for SCS variability, rough half of the summer SST variance remains to be explained, resulting possible from other processes such as internal variability of the SCS-western Pacific monsoon.

5. Summary and Discussion

[43] For the past decade, satellite remote sensing technology has been revolutionizing ocean observation, enabling us

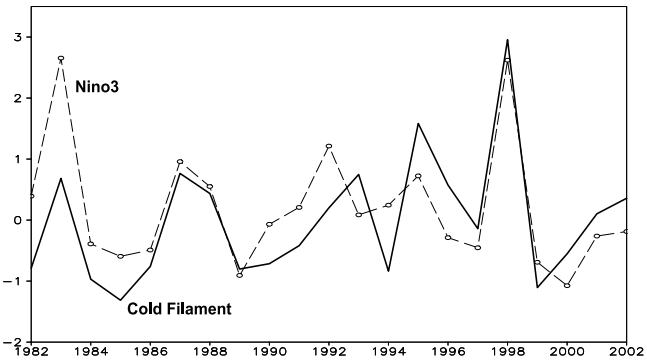

Figure 11. June–August cold filament index (solid) and January Nino3 index (dashed line with open circles), normalized by their respective RMS variance. RMS variance is 0.47 K for the cold filament and 1.36 K for the Nino3 index.

to make routine and high-resolution measurements of SST, SSH, ocean color, and surface winds over the world ocean. Taking advantage of these new satellite observations, we have investigated the seasonal and interannual variations of the SCS and the overlying atmosphere in boreal summer. On climatological mean, cold upwelled water is observed in June on the coast of South Vietnam after the onset of the southwest monsoon. In addition to the classical coastal upwelling mechanism, Ekman-pumping associated with a wind jet offshore seems also important for localizing the upwelling cooling on the coast east of Saigon. The upwelled cold water starts to spread northeastward offshore in July and August, forming a cold filament and causing a basin-wide mid-summer cooling. An anticyclonic circulation is found in the 8-year satellite climatology of SSH off the coast of South Vietnam, which is critical to the cold filament formation by advecting the cold coastal water offshore with its strong geostrophic currents. Satellite ocean-color observations corroborate the advective effect of this stationary SV Eddy and wind-induced offshore upwelling, revealing a high-chlorophyll tongue that heads offshore into the deep water and is roughly collocated with the cold filament.

[44] We have proposed a conceptual model that traces the cause of the SCS cold filament to orographic effects of Annam Cordillera. Under the background southwest monsoon in summer, the blockage by these mountains gives rise to a wind jet offshore southeast of Saigon. In addition to the evaporative cooling effect, this wind jet helps maintain the cold filament by inducing offshore upwelling on its northern flank. We also suggest that the Ekman downwelling on the southern flank of this wind jet forces the anticyclonic SV Eddy that advects cold coastal water offshore to form the cold filament.

[45] Interannual SST variance in summer shows a marked local maximum in the central SCS, suggesting that the cold filament plays an important role in regional climate variations. Wind changes are responsible for the interannual variability of the cold jet, through surface heat flux and Ekman pumping that modulates the strength and position of the SV Eddy. The cold filament becomes weaker or absent completely in years when the southwesterly winds in the SCS weaken. These wind changes are traced back to an

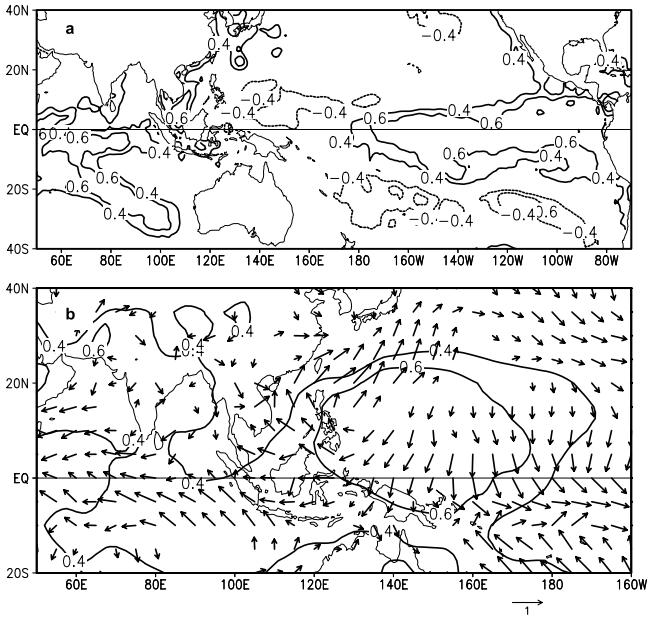

Figure 12. Lagged correlations with the summer SCS cold filament index: (a) SST, and (b) NCEP sea level pressure (contours) and surface wind velocity (vectors) in January the same year.

anomalous atmospheric high-pressure system over the northwestern tropical Pacific that develops concurrently with ENSO in the previous winter and persists into boreal summer.

[46] The southwesterly wind jet, the anticyclonic eddy off South Vietnam and the cold filament in the summer SCS join a growing number of examples that coastal/island mountains markedly affect both the atmosphere and the ocean. *Xie et al.* [2001] report far-reaching effects of mountains on Hawaii on the North Pacific Ocean and atmosphere, including a long streak of eastward countercurrent that results from the curls of the island wind wake flowing against the broad North Equatorial Current. *Kessler* [2002] show that the curl imposed by the wind jets blowing through gaps in the Central American cordillera imprints on the tropical North Pacific Ocean, producing geostrophic currents that are consistent with the Sverdrup balance. When the land orographic effect is imposed instead on the western side of the ocean basin as is in the SCS, the ocean response is likely to be highly nonlinear. Regarding such nonlinear ocean jets, we draw an analogy between the Great Whirl of the western Arabian Sea and the SV Eddy of SCS. Both are recurring climatological features that are forced by wind curls and involve nonlinear interaction with western boundary currents. At this stage, little is known about the mechanisms for the SV Eddy, a subject that needs further research.

[47] A major international field experiment took place over the SCS in summer 1998 that obtained comprehensive observations of the ocean and atmosphere [*Lau et al.*, 2000]. The summer of 1998, however, turns out to be rather abnormal for SCS, featuring a major warm event in the region following a strong El Niño as is described here and elsewhere. Our results call for future field campaigns to be conducted in a normal or cold year, targeting at a number of key processes to the mid-summer cooling identified here, including the mountain blockage effect, offshore wind jet, SV Eddy, cold filament and high-nutrient tongue in the central SCS.

[48] **Acknowledgments.** We would like to thank H. Xu and Z. Yu for discussion and sharing their numerical results, and J. Hafner for preparing satellite data sets. The merged SSH data set is obtained from the Collecte Localisation Satellites, France; TMI and QuikSCAT from Remote Sensing Systems; ERS from the Institut Français de Recherche pour l'Exploitation de la Mer; and AVHRR from JPL. This work is supported by NASA through its QuikSCAT and TRMM missions and grant NAG5-10045, by Frontier Research System for Global Change, by Natural Science Foundation of China (40240420564), Ministry of Science and Technology of China (2002AA639250), and Chinese Academy of Sciences (ZKCX2-SW-210). Part of Q. X.'s work is performed at IPRC on a Chinese Academy of Science Overseas Fellowship. IPRC contribution 210 and SOEST contribution 6169.

References

Annamalai, H., R. Murtugudde, J. Potemra, S.-P. Xie, P. Liu, and B. Wang, Coupled dynamics over the Indian Ocean: Spring initiation of the zonal mode, *Deep Sea Res., Part II*, *50*, 2305–2330, 2003.

Armstrong, E. M., and J. Vazquez-Cuervo, A new global satellite-based sea surface temperature climatology, *Geophys. Res. Lett.*, *28*, 4199–4202, 2001.

Chelton, D. B., S. K. Esbensen, M. G. Schlax, N. Thum, M. H. Freilich, F. J. Wentz, C. L. Gentemann, M. J. McPhaden, and P. S. Schopf, Observations of coupling between surface wind stress and sea surface temperature in the eastern tropical Pacific, *J. Clim.*, *14*, 1479–1498, 2001a.

Chelton, D. B., J. Ries, B. Haines, L.-L. Fu, and P. S. Callahan, Satellite altimetry, in *Satellite Altimetry and Earth Sciences*, edited by L.-L. Fu and P. S. Callahan, pp. 1–131, Academic, San Diego, Calif., 2001b.

Chu, P. C., C. Fan, C. J. Lozano, and J. L. Kerling, An airborne expendable bathythermograph survey of the South China Sea, May 1995, *J. Geophys. Res.*, *103*, 21,637–21,652, 1998.

Ducet, N., P. Y. Le Traon, and G. Reverdin, Global high-resolution mapping of ocean circulation from TOPEX/Poseidon and ERS-1 and -2, *J. Geophys. Res.*, *105*, 19,477–19,498, 2000.

Fang, W., G. Fang, P. Shi, Q. Huang, and Q. Xie, Seasonal structures of upper layer circulation in the southern South China Sea from in situ observations, *J. Geophys. Res.*, *107*, 3202, doi:10.1029/2002JC001343, 2002.

Hashizume, H., S.-P. Xie, W. T. Liu, and K. Takeuchi, Local and remote atmospheric response to tropical instability waves: A global view from space, *J. Geophys. Res.*, *106*, 10,173–10,185, 2001.

Ho, C.-R., N.-J. Kuo, Q. Zheng, and Y. S. Soong, Dynamically active areas in the South China Sea detected from TOPEX/POSEIDON satellite altimeter data, *Remote Sens. Environ.*, *71*, 320–328, 2000a.

Ho, C.-R., Q. Zheng, Y. S. Soong, N.-J. Kuo, and J.-H. Hu, Seasonal variability of sea surface height in the South China Sea observed with TOPEX/POSEIDON altimeter data, *J. Geophys. Res.*, *105*, 13,981–13,990, 2000b.

Huang, Q.-Z., W.-Z. Wang, Y. S. Li, and C. W. Li, Current characteristics of the South China Sea, in *Oceanology of China Sea*, edited by D. Zhou, Y.-B. Liang, and C. K. Tsebgm, pp. 39–47, Kluwer Acad., Norwell, Mass., 1994.

Hwang, C., and S.-A. Chen, Circulations and eddies over the South China Sea derived from TOPEX/Poseidon altimetry, *J. Geophys. Res.*, *105*, 23,943–23,965, 2000.

Kalnay, E., et al., The NCEP/NCAR 40-year re-analysis project, *Bull. Am. Meteorol. Soc.*, *77*, 437–471, 1996.

Kessler, W. S., Mean three-dimensional circulation in the northeast tropical Pacific, *J. Phys. Oceanogr.*, *32*, 2457–2471, 2002.

Kuo, N.-J., Q. Zheng, and C.-R. Ho, Satellite observation of upwelling along the western coast of the South China Sea, *Remote Sens. Environ.*, *74*, 463–470, 2000.

Lau, K.-M., H.-T. Wu, and S. Yang, Hydrologic processes associated with the first transition of the Asian Summer Monsoon: A pilot satellite study, *Bull. Am. Meteorol. Soc.*, *79*, 1871–1882, 1998.

Lau, K. M., et al., A report of the field operations and early results of the South China Sea Monsoon Experiment (SCSMEX), *Bull. Am. Meteorol. Soc.*, *81*, 1261–1270, 2000.

Liu, W. T., and X. Xie, Space-based observations of the seasonal changes of South Asian monsoons and oceanic response, *Geophys. Res. Lett.*, *26*, 1473–1476, 1999.

Liu, W. T., X. Xie, P. S. Polito, S.-P. Xie, and H. Hashizume, Atmospheric manifestation of tropical instability waves observed by QuikSCAT and

Tropical Rain Measuring Mission, *Geophys. Res. Lett.*, *27*, 2545–2548, 2000.

Nitta, T., Convective activities in the tropical western Pacific and their impact on the Northern Hemisphere summer circulation, *J. Meteorol. Soc. Jpn.*, *65*, 373–390, 1987.

Nonaka, M., and S.-P. Xie, Co-variations of sea surface temperature and wind over the Kuroshio and its extension: Evidence for ocean-to-atmospheric feedback, *J. Clim.*, *16*, 1404–1413, 2003.

Ose, T., Y. Song, and A. Kitoh, Sea surface temperature in the South China Sea: An index for the Asian monsoon and ENSO system, *J. Meteorol. Soc. Jpn.*, *75*, 1091–1107, 1997.

Pohlmann, T., A three-dimensional circulation model of the South China Sea, in *Three-Dimensional Models of Marine and Estuarine Dynamics*, edited by J. J. Nihoul and B. M. Jamart, pp. 245–268, Elsevier Sci., New York, 1987.

Qu, T., Upper-layer circulation in the South China Sea, *J. Phys. Oceanogr.*, *30*, 1450–1460, 2000.

Qu, T., Role of ocean dynamics in determining the mean seasonal cycle of the South China Sea surface temperature, *J. Geophys. Res.*, *106*, 6943–6955, 2001.

Reynolds, R. W., and T. M. Smith, Improved global sea surface temperature analyses using optimal interpolation, *J. Clim.*, *7*, 929–948, 1994.

Schott, F. A., and J. P. McCreary, The monsoon circulation of the Indian Ocean, *Prog. Oceanogr.*, *51*, 1–123, 2001.

Shaw, P.-T., and S.-Y. Chao, Surface circulation in the South China Sea, *Deep Sea Res., Part I*, *41*, 1663–1683, 1994.

Wang, B., R. Wu, and X. Fu, Pacific-East Asian teleconnection: How does ENSO affect East Asian climate?, *J. Clim.*, *13*, 1517–1536, 2000a.

Wang, D., Q. Xie, Y. Du, W.-Q. Wang, and J. Chen, The 1997–1998 warm event in the South China Sea, *Chin. Sci. Bull.*, *47*, 1221–1227, 2002.

Wang, W. Q., D. Wang, and Y. Qi, Large-scale characteristics of interannual variability of sea surface temperature in the South China Sea, *Acta Oceanol. Sin.*, *22*, 8–16, 2000b.

Wei, Z., G. H. Fang, B.-H. Choi, Y. Fang, and Y. He, Sea surface height and transport stream function of the South China Sea from a variable-grid global ocean circulation model, *Sci. China D*, *46*, 139–148, 2003.

Wentz, F. J., C. Gentemann, D. Smith, and D. Chelton, Satellite measurements of sea surface temperature through clouds, *Science*, *288*, 847–850, 2000.

Wyrtki, K., Physical oceanography of the Southeast Asian waters: Scientific results of marine investigations of the South China Sea and the Gulf of Thailand, *NAGA Rep. 2*, 195 pp., Scripps Inst. of Oceanogr., La Jolla, Calif., 1961.

Xie, P., and P. A. Arkin, Analyses of global monthly precipitation using gauge observations, satellite estimates, and numerical model predictions, *J. Clim.*, *9*, 840–858, 1996.

Xie, Q., W. Q. Wang, and Q. Mao, Comparison among four kinds of data of sea surface wind stress in the South China Sea, *Acta Oceanol. Sin.*, *21*, 263–273, 2002a.

Xie, S.-P., M. Ishiwatari, H. Hashizume, and K. Takeuchi, Coupled ocean-atmospheric waves on the equatorial front, *Geophys. Res. Lett.*, *25*, 3863–3866, 1998.

Xie, S.-P., W. T. Liu, Q. Liu, and M. Nonaka, Far-reaching effects of the Hawaiian Islands on the Pacific Ocean-atmosphere, *Science*, *292*, 2057–2060, 2001.

Xie, S.-P., H. Annamalai, F. A. Schott, and J. P. McCreary, Origin and mechanisms of South Indian Ocean climate variability, *J. Clim.*, *15*, 864–878, 2002b.

Xu, X., Z. Qiu, and H. Chen, The general descriptions of the horizontal circulation in the South China Sea, in *Proceedings of the 1980 Symposium of the Chinese Society of Marine Hydrology and Meteorology*, pp. 119–127, Sci. Press, Beijing, 1982.

Yang, H., Q. Liu, Z. Liu, D. Wang, and X. Liu, A general circulation model study of the dynamics of the upper ocean circulation of the South China Sea, *J. Geophys. Res.*, *107*, 3085, doi:10.1029/2001JC001084, 2002.

W. T. Liu, Jet Propulsion Laboratory 300-323, Pasadena, CA 91109-8099, USA. (liu@pacific.jpl.nasa.gov)

D. Wang and Q. Xie, Laboratory of Tropical Marine Environmental Dynamics, South China Sea Institute of Oceanology, Chinese Academy of Sciences, Guangzhou 510301, China. (dxwang@scsio.ac.cn; gordonxie@scsio.ac.cn)

S.-P. Xie, International Pacific Research Center, SOEST, University of Hawaii, Honolulu, HI 96822, USA. (xie@hawaii.edu)